Received: 19 October 2024 | Revised: 29 January 2025 | Accepted: 17 February 2025

DOI: 10.1002/ardp.202400821

ARCH PHARM DPhG
Archiv der Pharmazie

FULL PAPER

Design, synthesis of novel thiazole-thiomorpholine derivatives and evaluation of their anticancer activity via in vitro and in silico studies

Sam Dawbaa[1,2] | Asaf Evrim Evren[1,3] | Demokrat Nuha[1,4] | Halide Edip Temel[5] | Gülşen Akalin Çiftçi[5] | Leyla Yurttaş[1]

[1]Department of Pharmaceutical Chemistry, Faculty of Pharmacy, Anadolu University, Eskişehir, Turkey

[2]Department of Pharmacy, Faculty of Medical Sciences, Thamar University, Dhamar, Yemen

[3]Department of Pharmacy Services, Vocational School of Health Services, Bilecik Şeyh Edebali University, Bilecik, Turkey

[4]Faculty of Pharmacy, University of Business and Technology, Prishtina, Kosovo

[5]Department of Biohemistry, Faculty of Pharmacy, Anadolu University, Eskişehir, Turkey

Correspondence
Sam Dawbaa, Department of Pharmacy, Faculty of Medical Sciences, Thamar University, Dhamar 87246, Yemen.
Email: dawbaa655@anadolu.edu.tr and sdawbaa@tu.edu.ye

Funding information
Anadolu University Scientific Research Project, Eskisehir, Turkey, Grant/Award Number: 2105S098

Abstract

Continuous efforts are carried out to find new cancer treatments. Compounds including thiazole or thiomorpholine rings showed favorable biological activities for various diseases including cancer. In this study, a new series of 4-(4-{[2-(4-phenylthiazol-2-yl)hydrazono]methyl}phenyl)thiomorpholine derivatives were synthesized and tested in vitro for their anticancer activity. Twelve compounds including various 4-phenylthiazol and a single 4-(2-naphthyl)thiazole derivatives were synthesized and analyzed by ^{1}H-nuclear magnetic resonance (NMR), ^{13}C-NMR, and high-resolution mass spectrometry (HRMS). The cytotoxic effects of the compounds were tested on the A549 lung cancer cell line and the L929 healthy cell line. Six compounds (**3a**, **3b**, **3c, 3d**, **3e**, and **3f**) showed better inhibitory activity against A549 cells than the reference drug cisplatin. Compound **3f** (4-CH_3 phenyl derivative) was the most potent with an IC_{50} of 3.72 µM. The cytotoxic activity against the healthy cell line L929 was evaluated and all of the tested compounds displayed IC_{50} values of more than 500 µM, indicating a selectivity toward the cancer cell line A549. Activity against matrix metalloproteinase-9 was also tested and the result indicated a %inhibition of 68.02 and 52.77 for compounds **3g** and **3j**, respectively. In silico evaluation was achieved via Density Functional Theory calculations and molecular dynamic simulations and the results were in line with those of the in vitro tests.

KEYWORDS
A549, MDS, MMP-9, thiazole, thiomorpholine

1 | INTRODUCTION

Cancer is a broad term for a disease that can impact various organs and comes in many forms. Each year, it causes the deaths of between 100 and 300 individuals per 100,000 people worldwide.[1] Current anticancer drugs operate through a variety of mechanisms, each associated with different side effects.[2,3] Consequently, the goal of designing small molecules as anticancer agents is to develop more selective treatments that target tumor cells while minimizing adverse effects. Research has shown that incorporating various heterocyclic rings as substituents in certain pharmacophores can enhance anticancer activity.[4–6]

In new design approaches, the focus is on modifying existing molecules or exploring the pharmacophore structures of new

compounds. A review of current anticancer drugs reveals that the thiazole ring plays a significant role in cancer therapy. It is likely a preferred structural unit due to its compatibility with biological systems, which may lead to a reduced incidence of adverse reactions.[7] Moreover, the therapeutic properties of the thiazole ring extend beyond cancer treatment; it shows efficacy against HIV infections, bacteria, schizophrenia, inflammation, hypertension, and allergies. Natural thiazole derivatives, particularly those extracted from seafood, also exhibit antineoplastic and cytotoxic activities.[8–14] One well-known drug that includes a thiazole ring is bleomycin, recognized for its potent antitumor effects against lymphoma, head and neck cancers, and germ cell tumors.[15]

Thiomorpholine is a hexagonal cyclic compound with unique properties, including high water solubility, weak basicity, electron-donating activity, and low biological toxicity.[16] These characteristics make thiomorpholine a valuable structural unit for enhancing the pharmacokinetic and pharmacodynamic properties of drug candidates. Several studies have indicated that the thiomorpholine ring contributes to a range of biological activities, including anticancer, antitubercular, and antimicrobial effects.[17–19] The limited biological data available on thiomorpholine highlights the need for further investigation into this compound. Various studies indicate that thiomorpholine exhibits significant anticancer activity, with some findings suggesting that this effect is selective for tumor cells.[19–22]

This study involved the design of thiazole derivatives that incorporate a thiomorpholine ring, aimed at addressing the demand for new selective anticancer drugs with reduced adverse effects compared with current treatments. New 4-[4-[(2-(4-substituted thiazol-2-yl)hydrazinylidene)methyl]phenyl]thiomorpholine (**3a–3l**) derivatives were synthesized and analyzed using nuclear magnetic resonance (NMR) and high-resolution mass spectrometry (HRMS) techniques. The anticancer activities of the compounds were investigated and the results were analyzed via in silico studies.

2 | RESULTS AND DISCUSSION

2.1 | Chemistry

The compounds **3a–3l** were synthesized as summarized in Scheme 1.

In this study, we synthesized 12 new compounds which included the 4-(4-{[2-(thiazol-2-yl)hydrazono]methyl}phenyl)thiomorpholine (**3a–3l**) nucleus in their core structures. The synthesis steps are illustrated in Scheme 1. In the first step, 4-fluorobenzaldehyde and thiomorpholine were reacted in DMF for 24 h at 150°C to obtain 4-thiomorpholinobenzaldehyde (**1**).[23] Next, compound **1** and hydrazine carbothioamide were reacted for 3 h at 80°C to obtain 2-(4-thiomorpholinobenzylidene)hydrazinecarbothioamide (**2**).[23] In the final step, compound **2** and 2-bromo-1-phenylethanone derivatives were reacted in ethanol to gain the final products 4-(4-{[2-(thiazol-2-yl)hydrazono]methyl}phenyl)thiomorpholine derivatives (**3a–3l**) as shown in Scheme 1. The structures of the synthesized compounds (**3a–3l**) were confirmed by ^{1}H-NMR, ^{13}C-NMR, and HRMS. In the ^{1}H-NMR spectra, the aromatic and aliphatic regions' peaks were seen at their expected chemical shifts. Similarly, ^{13}C-NMR spectra displayed the predicted peaks at the estimated shifts. The mass spectra (ESI-MS), and the compounds' [M+1] peaks were consistent with their predicted molecular formula (**3a–3l**).

The ^{1}H-NMR spectra showed a broad singlet peak at δ = 2.08–4.01 ppm for thiomorpholine-$\underline{C}_2$ and $\underline{C}_6$ protons. Thiomorpholine-$\underline{C}_3$ and $\underline{C}_5$ proton was observed at δ = 3.62–4.33 ppm as a broad singlet peak. Methylene hydrazine (N–N=$\underline{C}$H) proton was

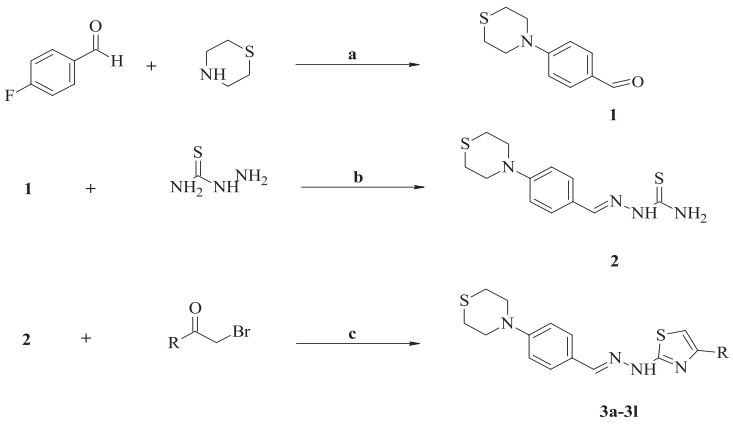

Comp.	R
3a	4-F phenyl
3b	4-Cl phenyl
3c	4-NO_2 phenyl
3d	phenyl
3e	4-CN phenyl
3f	4-CH_3 phenyl
3g	4-OCH_3 phenyl
3h	3-Cl phenyl
3i	3-OCH_3 phenyl
3j	3-NO_2 phenyl
3k	3-F phenyl
3l	2-naphthyl

SCHEME 1 The synthesis diagram of the compounds **3a–3l**. Reagents and conditions: (a) K_2CO_3, DMF, reflux, 24 h; (b) EtOH, reflux; (c) EtOH, reflux.

observed at 7.93–8.37 ppm as a singlet peak. A broad singlet peak at δ = 10.44–10.53 ppm indicates the N–H proton. The appearance of a pair of singlets, doublets, triplets, and/or multiplets at σ 6.71–8.71 ppm was due to the aromatic protons of the aromatic rings. The ^{13}C-NMR spectra showed signals at δ = 25.27–34.16 ppm for thiomorpholine-$\underline{C}_2$ and $\underline{C}_6$ carbon, δ = 38.16–51.77 ppm for thiomorpholine-$\underline{C}_3$ and $\underline{C}_5$ carbon, δ = 101.78–168.68 ppm for aromatic carbons. The mass spectral (HRMS) [M ± 1] peaks were consistent with the calculated molecular weights of the target compounds (**3a–3l**). The infrared (IR) spectral analysis revealed that the N–H stretching band associated with the amino group in compounds **3a–3l** was absent in most instances; however, it was detected around 3300 cm^{-1} in some compounds. Aromatic C–H stretching occurred in the range of 3082–3050 cm^{-1}, while aliphatic C–H stretching was observed between 2995 and 2814 cm^{-1}. Bands corresponding to the C=C and C=N bonds were identified between 1622 and 1357 cm^{-1}, and C–N bond bands were detected in the range of 1281–1011 cm^{-1}. Additionally, the deformation bands of the substituted benzene ring appeared as complex patterns within the fingerprint region of 635–993 cm^{-1}.

2.2 | Biology

The cytotoxic effects of the compounds were tested on the A549 lung cancer cell line and the L929 healthy cell line. The results presented in Table 1 in μM unit indicated that the compounds exhibited inhibition concentrations ranging from 3.72±1.09 μM to >500 μM. The IC_{50} of cisplatin, used as a reference drug, was determined to be 38.31±5.88 μM. Compounds **3a–3f** demonstrated excellent cytotoxic effects, showing greater potency than cisplatin. Furthermore, all compounds showed negligible cytotoxic effects against healthy cell line L929, even at the highest concentration tested, indicating selectivity. The remaining compounds were concluded to be inactive against the A549 cell line.

The molecules are differentiated due to the aryl group in the fourth position of the thiazole ring. Among the substituted phenyl derivatives and the derivatives containing the naphthalene ring, compound **3f** (4-methyl phenyl derivative) showed the most potent activity with an IC_{50}:3.72 μM. The second most active candidate was compound **3d** (IC_{50}:4.87 μM), which is the unsubstituted phenyl derivative. The compounds **3c** (4-nitrophenyl), **3e** (4-cyanophenyl), **3b** (4-chlorophenyl), and **3a** (4-fluorophenyl), also demonstrated higher cytotoxicity than cisplatin.

The inhibitory effects of the synthesized compounds on matrix metalloproteinase (MMP)-9 were investigated to better understand the mechanism of their anticancer activity. The results, shown in Table 2 as percent inhibition at a dosage of 100 μM, revealed that compounds **3g** and **3j** demonstrated the highest activity, with inhibition rates of 68.02% and 52.77%, respectively. The other compounds showed MMP-9 inhibition rates ranging from 9.4% to 27.73%, indicating relatively low levels of activity. In comparison, the standard drug NNGH (*N*-isobutyl-*N*-(4-methoxyphenylsulfonyl)glycyl hydroxamic acid) exhibited a percentage inhibition of 92.84% at a concentration of 1.3 μM.

2.3 | Absorption, Distribution, Metabolism, and Excretion (ADME) parameters

In silico ADME research of compounds **3a–3l** and reference pharmaceuticals was performed using the SwissADME online tool, and

TABLE 1 IC_{50} values of compounds 3a–3l on cell lines A549 and L929.

Compounds	IC_{50} (μM) A549	L929
3a	28.27 ± 0.55	>500
3b	21.43 ± 4.89	>500
3c	7.93 ± 0.12	>500
3d	4.87 ± 1.00	>500
3e	18.17 ± 2.57	>500
3f	3.72 ± 1.09	>500
3g	>500	>500
3h	339.7 ± 79.48	>500
3i	>500	>500
3j	>500	>500
3k	>500	>500
3l	>500	>500
Cisplatin	38.31 ± 5.88	-

Abbreviation: -, not determined.

TABLE 2 The percent inhibitions of 3a–3l compounds on MMP-9 enzyme.

Compounds (100 μM)	MMP-9% inhibition
3a	----
3b	----
3c	----
3d	----
3e	25.84 ± 3.90
3f	23.92 ± 2.55
3g	68.02 ± 1.72
3h	27.73 ± 3.30
3i	----
3j	52.77 ± 1.51
3k	----
3l	9.40 ± 1.22
NNGH (1.3 μM)	92.84 ± 2.46

Abbreviation: ----, not determined; MMP-9, matrix metalloproteinase-9.

important five physicochemical characteristics were identified.[24] Table 3 displays the values for hydrogen bond acceptors (HBA), hydrogen bond donors (HBD), topological polar surface area (TPSA), lipophilicity descriptor (Log P), water solubility descriptor (Log S), skin permeation descriptor (Log K_p), gastrointestinal absorption (GIA), and other parameters. According to Lipinski's "Rule of 5," all of the synthesized compounds have good membrane permeability (BBB/GI), log P (3.59–5.07) ≤6, number of HBA (2–4) ≤10, molecular weight ≤500, and the number of HBD (1) ≤5. The compounds' pharmacophore or drug-like properties indicated that they all follow and satisfy Lipinski's rule, with all attributes falling within an acceptable range.[25] The synthesized molecules are expected to have a favorable pharmacokinetic profile.

2.4 | Density Functional Theory (DFT) studies

The examination of the structure, stability, and characteristics of active compounds **3a**, **3b**, **3f**, and **3g** involved the application of DFT-based global reactivity descriptors. These descriptors have been widely utilized to assess the reactivity and site selectivity of various biomolecules. The three-dimensional structure of the investigated compounds was analyzed using theoretical methods to generate optimized molecular structures. By employing DFT optimization, the structures of the most active compounds (**3a**, **3b**, **3f**, and **3g**) were obtained, and no imaginary frequency was observed when utilizing the B3LYP/6-31 G (d, p) basis set. Figure 1 illustrates the optimized structures of the active compounds **3a**, **3b**, **3f**, and **3g**.

At the B3LYP/6-31 G (d, p) level, the optimized geometries' frontier molecular orbitals were analyzed. The determination of chemical reactivity, optical polarizability, chemical softness, hardness, and molecular electrical transport properties for any chemical system relies on the energy difference between the highest occupied molecular orbital (HOMO) and the lowest unoccupied molecular orbital (LUMO). Table 4 presents the energies of the frontier molecular orbitals and the energy difference between HOMO and LUMO. Stability can be inferred for compounds **3a**, **3b**, **3f**, and **3g** as their HOMO and LUMO values are negative (Figure 2). The experimental findings support the chemical properties outlined in Table 4, indicating that compound **3c** exhibits greater activity compared with other compounds. Additionally, compound **3g** possesses a low ionization potential (I) value, while compound **3c** exhibits a high electron affinity (A) value, both associated with HOMO and LUMO energy. Consequently, compound **3g** demonstrates nucleophilic character, whereas the **3c** molecule exhibits enhanced electrophilic character.

Among the tested compounds, compound **3c** stands out with an electronegativity value of 0.1371 eV, indicating higher electronegativity, and a nucleophilic character of 0.1746 eV, surpassing the other compounds. Furthermore, the chemical hardness-softness (η, S) values play a role in assessing the intramolecular charge transfer within molecular structures. It is noteworthy that compound **3c** exhibits high softness (S) and low hardness (η) values, signifying its distinctive characteristics.

The analysis of the molecular electrostatic potential (MEP) is essential for understanding the charge distribution within three-dimensional molecules, as well as for evaluating ligand binding and hydrogen bonding with biomolecules.[26] Figure 3 illustrates the MEP mapping results for the active compounds. MEP visualization utilizes a color scheme: red represents areas with a partial negative charge and an electron-rich nature, blue indicates regions with a partial positive charge and an electron-deficient nature, yellow denotes moderately electron-rich regions, and green signifies neutral regions.[27]

2.5 | Molecular mechanics studies

The molecular docking study (Figure 4), reveals that the 4-methoxyphenyl moiety of compound **3g** is positioned within the active pocket of the enzyme, while the N-phenylthiomorpholine moiety interacts with the enzyme's hydrophobic side. This particular arrangement results in the occupation of His226, a critical amino acid for enzyme stability, through π–π stacking interactions. Additionally, the methoxy and phenyl groups of **3g** formed aromatic hydrogen bonds with residues Tyr245, Met247, and Tyr248. Another aromatic hydrogen bond is observed between the phenyl group attached to thiomorpholine and Ala191. Furthermore, an ionic interaction was established between the N1 of the hydrazone and Mn2000, which plays a significant role in inhibiting the MMP enzyme family.[28–30] Consistent with previous studies,[31,32] the experimental results show comparable binding modes, supporting the validity of the docking results. In addition, as shown in Figure 4c, these findings suggest that **3g** occupies two major binding pockets.[33,34] To enhance its activity, the structure of **3g** should be modified to interact more effectively with the loop region (seq. 233-257). Overall, these results clarify the potential binding mode between **3g** and the MMP-9 enzyme.

To gain a deeper understanding of the environmental changes over time, a molecular dynamics simulation (MDS) study was conducted based on the docking results. The stability plots from the MDS results (Figure 5a–c), revealed that the radius of gyration (Rg) value for the ligand ranged between 6.15 and 6.30 Å. Additionally, the maximum and minimum root-mean-square deviation (RMSD) values for the protein remained within an acceptable range of 1–3 Å throughout the simulation. Specifically, the RMSD value of the ligand when fitted to itself ranged from 0.25 to 0.75 Å, while the RMSD value of the ligand when fitted to the protein varied between 0.50 and 2.0 Å. The RMSD peaks observed in Figure 5c did not demonstrate significant changes during the simulation, with variations of no more than 0.25 Å after 20 ns. Conversely, the root-mean-square fluctuation (RMSF) peaks for compound **3g** interacting with the enzyme's loop amino acids (indicated by the white area in the figure) remained below 1 Å. These findings indicate that stability was maintained throughout the duration of the simulation.

The results of the MDS (Figure 6a–c and online video, https://youtu.be/QLCHnH-2eDo) indicate that interactions between the histidine residues (seq. 226, 230, and 236) and Glu227 were

TABLE 3 Physicochemical, pharmacokinetic, and medicinal chemistry properties of the final compounds (by SwissAdme) 3a–3l.

Physicochemical properties					Pharmacokinetics			Medicinal chemistry	
	HBA	HBD	TPSA	Log $P_{o/w}$	Log S	GIA	Log K_p	RoF (V)	SA
3a	3	1	94.06	4.48	−6.93	High	−5.03	Yes (0)	3.38
3b	2	1	94.06	4.61	−7.48	High	−4.76	Yes (0)	3.35
3c	4	1	139.88	3.59	−7.61	Low	−5.39	Yes (0)	3.48
3d	2	1	94.06	4.23	−6.83	High	−4.99	Yes (0)	3.36
3e	3	1	117.85	3.95	−7.04	High	−5.34	Yes (0)	3.47
3f	2	1	94.06	4.49	−7.21	High	−4.82	Yes (0)	3.48
3g	3	1	103.29	4.16	−6.99	High	−5.20	Yes (0)	3.43
3h	2	1	94.06	4.68	−7.48	High	−4.76	Yes (0)	3.34
3i	3	1	103.29	4.17	−6.99	High	−5.20	Yes (0)	3.46
3j	4	1	139.88	3.60	−7.62	Low	−5.39	Yes (0)	3.56
3k	3	1	94.06	4.46	−6.93	High	−5.03	Yes (0)	3.38
3l	2	1	94.06	5.07	−8.13	High	−4.41	Yes (0)	3.59
R1	9	6	181.62	−0.40	−3.64	Low	−8.83	Yes (1)	5.17
R2	7	1	81.65	0.88	−1.63	High	−7.92	Yes (0)	2.91

Abbreviations: GIA, gastrointestinal absorption; HBA, H-bond acceptor; HBD, H-bond donor; Log $P_{o/w}$, *Consensus* Log $P_{o/w}$ (Average of all five predictions); Log S, water solubility; Log K_p, skin permeation (cm/s); R1, Tetracycline; R2, Fluconazole; RoF (V), Rule of Five (violation number); SA, synthetic accessibility from 1 (very easy) to 10 (very difficult); TPSA, topologic polar surface area (Å²).

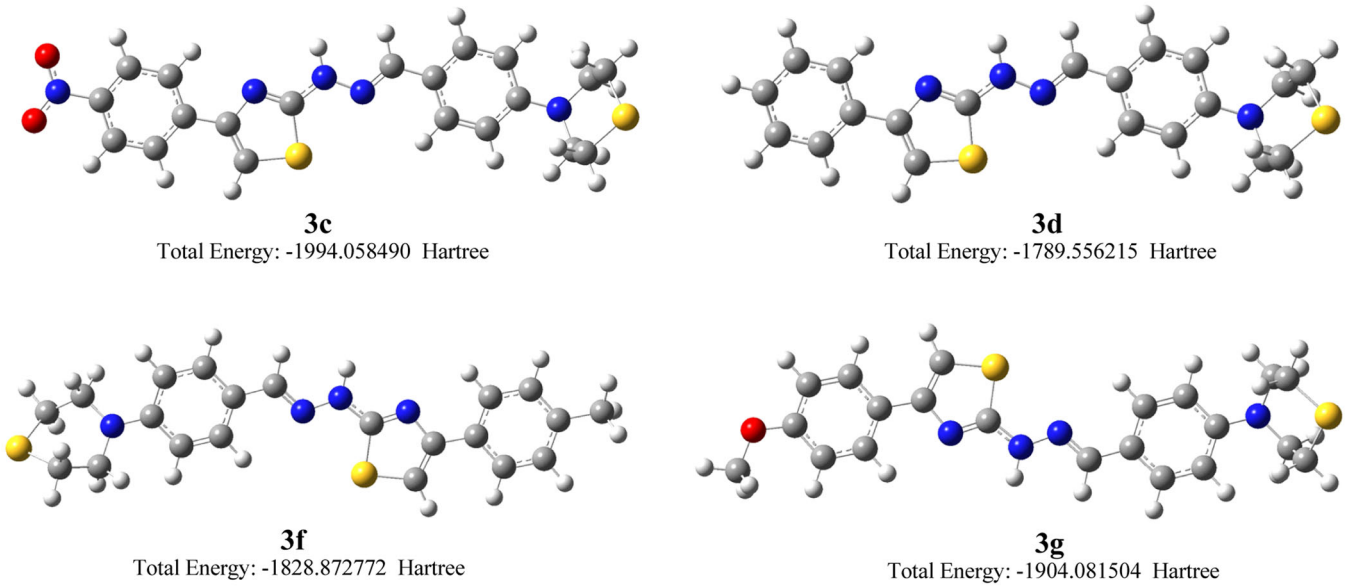

FIGURE 1 Optimized molecular structures and total energy values of active compounds.

TABLE 4 Some reactivity parameters of the most active compounds.

Compounds	E_{HOMO} (eV)	E_{LUMO} (eV)	ΔE (eV)	I (eV)	A (eV)	χ (eV)	η (eV)	S (eV^{-1})	μ (eV)	ω (eV)
3c	−0.1910	−0.0833	0.1077	0.191	0.0833	0.1371	0.0538	9.2850	−0.1371	0.1746
3d	−0.1806	−0.0445	0.1361	0.1806	0.0445	0.1125	0.0681	7.3475	−0.1125	0.0931
3f	−0.1780	−0.0418	0.1362	0.178	0.0418	0.1099	0.0681	7.3421	−0.1099	0.0887
3g	−0.1767	−0.0426	0.1341	0.1767	0.0426	0.1096	0.0671	7.4571	−0.1096	0.0897

observed through metal-mediated ionic bonds. The thiazole nitrogen and the N1 of the hydrazone in compound **3g** appear to be crucial for its inhibitory activity. Therefore, it is suggested that the thiazolohydrazone moiety be identified as a pharmacophore responsible for inhibiting the MMP-9 enzyme.

Additionally, the 4-methoxyphenyl group and thiazole directly interacted with His226 and His336, respectively, through π–π stacking. Aromatic hydrogen bonds were formed with the residues Tyr179, Gly186, Ala191, Glu227, Pro246, and Tyr248; however, more frequent hydrogen bonding was observed with Ala191, Glu227, and Tyr248. These findings suggest that the thiazolohydrazone moiety promotes inhibitory activity due to its interactions with Zn and the histidine residues (seq. 226, 230, and 236).

In comparison to the molecular docking results, compound **3g** effectively localized within the binding region and occupied two major pockets of the enzyme. This localization supports the maintenance of complex stability throughout the simulation. Nevertheless, the lack of interactions with one of the important loop regions (seq. 233–257), aside from Tyr248, resulted in reduced inhibitory activity relative to existing MMP-9 drugs. Therefore, for future studies, it is recommended that subsequent modifications focus on expanding the current molecules to facilitate continuous interaction with this region.

Investigating the **3g**-MMP-9 complex revealed a potential binding mode, highlighting that thiazole and hydrazone moieties significantly influence key residues (e.g., Zn2000, His226, His236).

3 | CONCLUSION

The current study aimed to synthesize hybrid thiomorpholine-thiazole derivatives with potential anticancer activity. The synthesized derivatives were modified by altering the substituents at C-3 and C-4 of the phenyl ring, which is attached to C-4 of the thiazole ring. Results from in vitro anticancer activity evaluations on the A549 lung cancer cell line indicated that the 4-substituted phenyl derivatives exhibited greater activity than the reference compound, cisplatin. Notably, the electron-donating substituent 4-CH_3 (**3f**) was the most active, followed closely by the unsubstituted phenyl derivative (**3d**). In contrast, the 4-OCH_3 derivative (**3g**) displayed poor activity, as did the 3-substituted phenyl derivatives. These findings highlight the importance of favorable substitutions at C-4 of the phenyl ring for enhanced activity. Additionally, increasing the size of the ring led to a decrease in activity, as seen with the naphthalene derivative (**3l**). In terms of cytotoxic effects on the

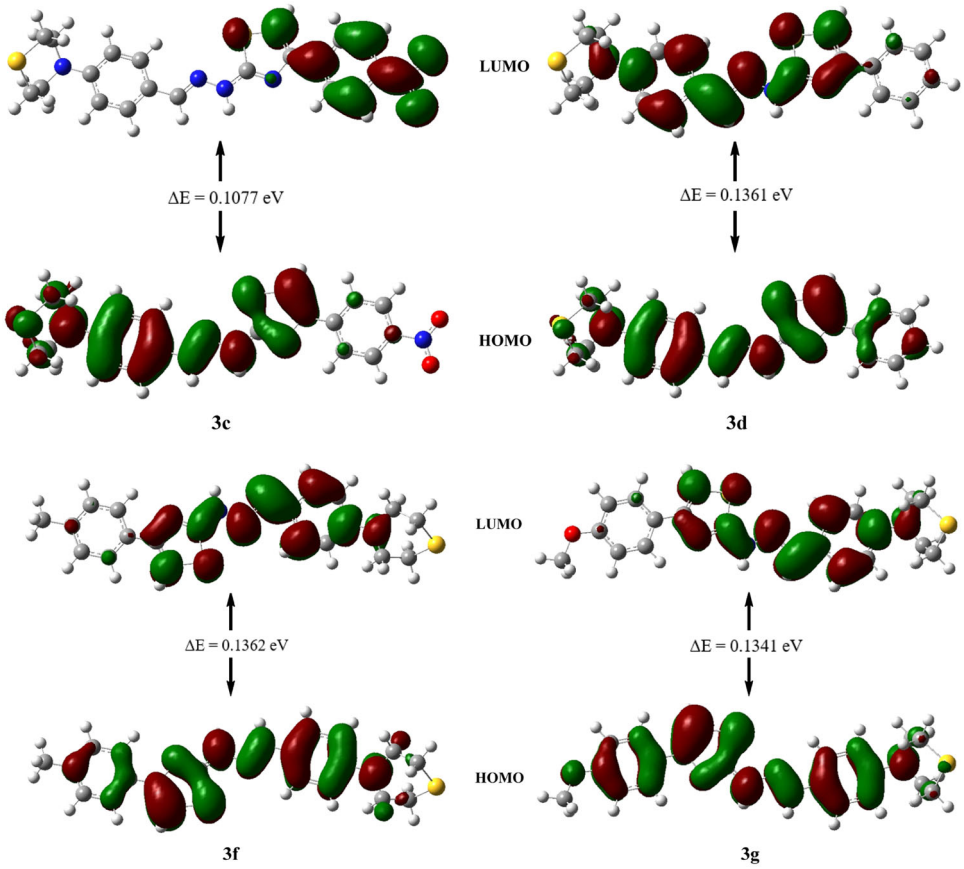

FIGURE 2 Highest occupied molecular orbital (HOMO)-lowest unoccupied molecular orbital (LUMO) diagrams of the active compounds.

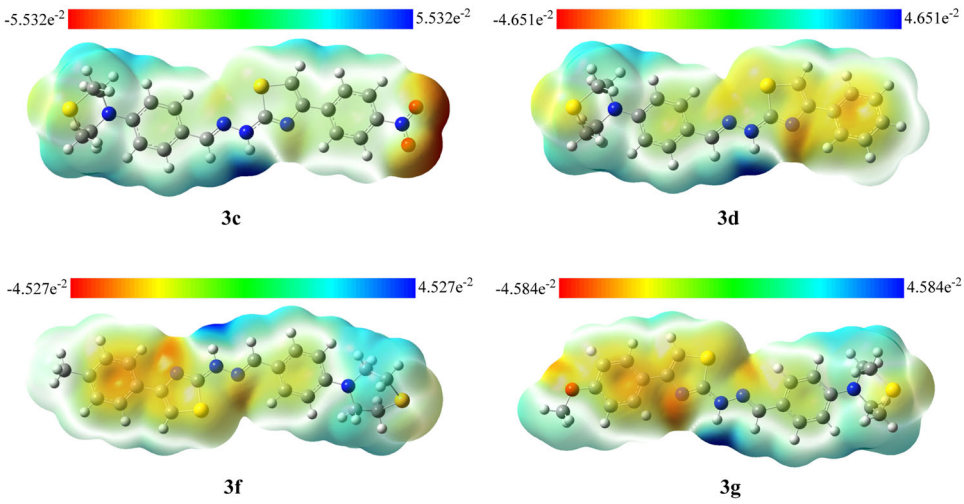

FIGURE 3 Molecular electrostatic potential (MEP) surfaces presentation of the active compounds.

healthy L929 cell line, all synthesized compounds demonstrated promising safety, showing a significant IC_{50} difference compared with the effective IC_{50} values on the A549 cell line. Despite its limited activity against the A549 cell line, compound **3g** exhibited the highest activity in the MMP-9 test, while compound **3j** showed the second highest activity following compound **3g** in inhibiting MMP-9. The MDS study results elucidated the role of the thiazole nitrogen and N1 of the attached hydrazone moiety in the activity of compound **3g** for MMP-9 inhibition. Although the contribution of the thiomorpholine is still unclear, it was concluded that the thiazole ring, along with the hydrazone functionality, is a significant structural feature in inhibiting MMP-9.

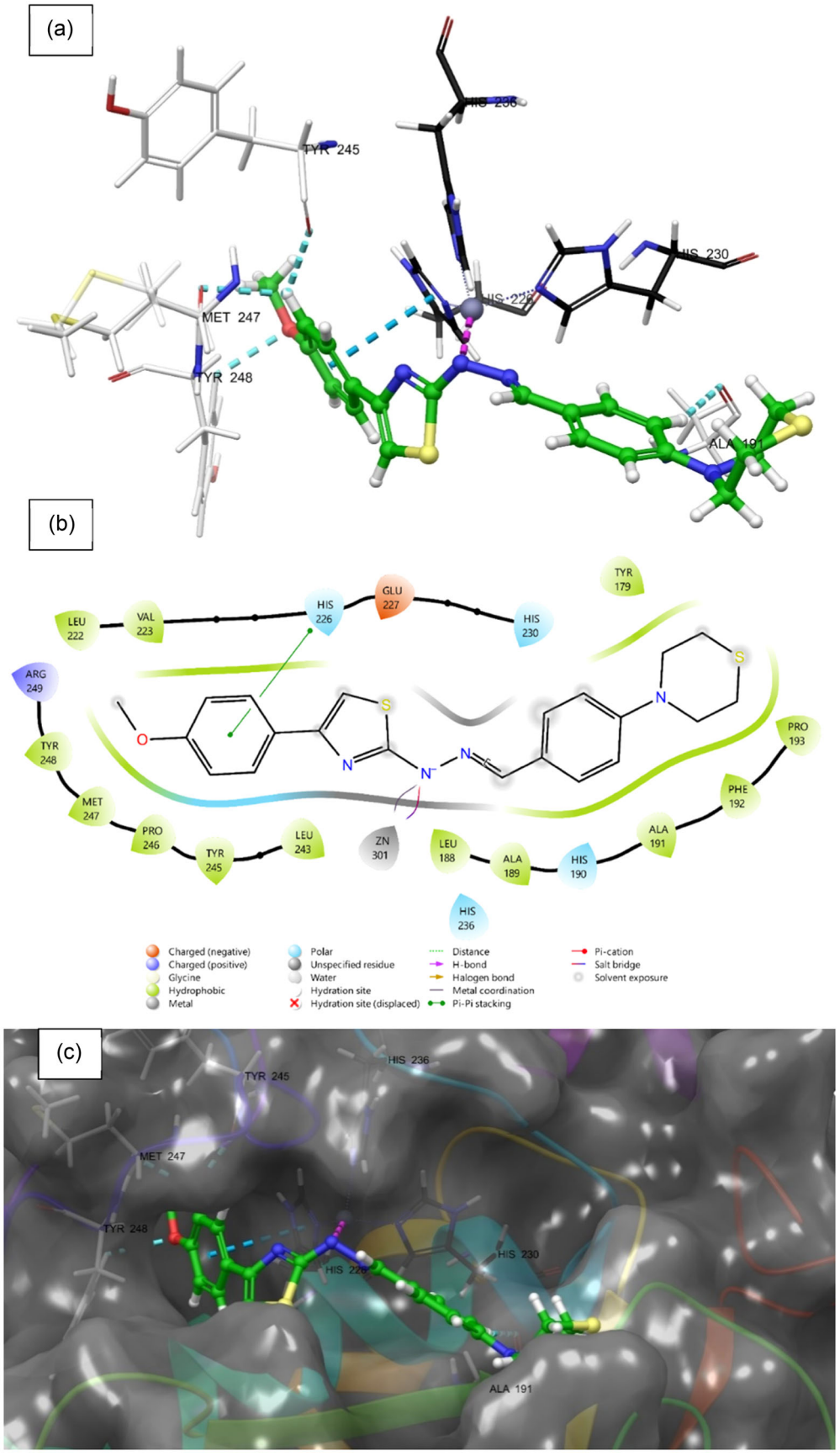

FIGURE 4 Three-dimensional (3D) (a) and two-dimensional (2D) (b) molecular docking pose of **3g**-matrix metalloproteinase (MMP)-9 enzyme complex. (c) 3D poses with protein surfaces.

FIGURE 5 Stability plots of the molecular dynamics simulation (MDS) results for **3g**-matrix metalloproteinase-9 (MMP-9) complex. The stability properties (Rg, root-mean-square deviation (RMSD), and root-mean-square fluctuation (RMSF) plots, respectively) are shown in (a), (b), and (c) sections, respectively.

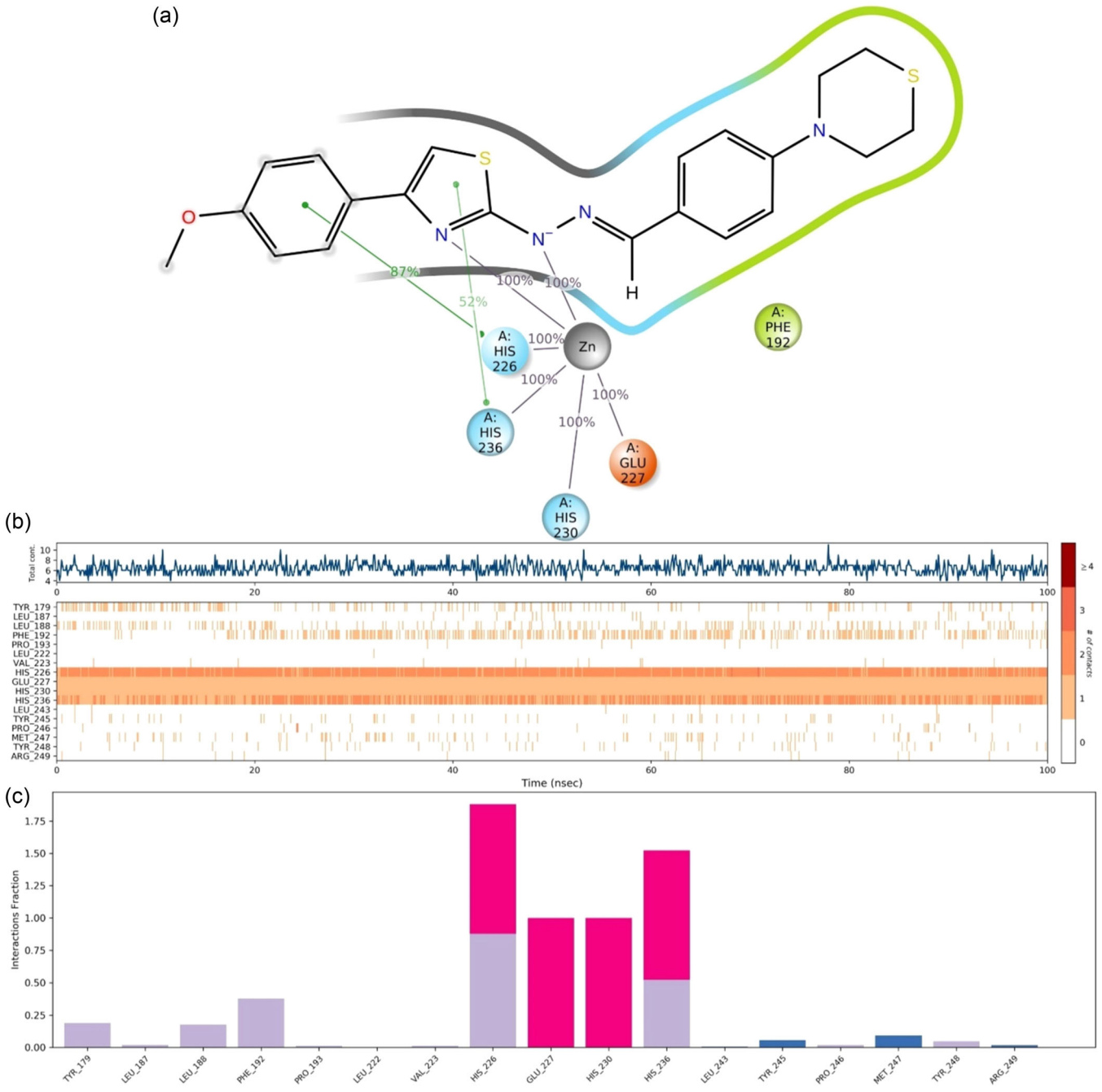

FIGURE 6 The interaction properties of molecular dynamics simulation (MDS) result. (a) Two-dimensional (2D) interaction pose with connection strength (cutoff = 0.2) at the active region of matrix metalloproteinase-9 (MMP-9), (b) interaction fraction–residue diagram, and (c) number of interactions–interaction types–time plot of **3g**.

4 | EXPERIMENTAL

4.1 | Chemistry

4.1.1 | General

All chemicals used in the syntheses were purchased either from Merck Chemicals (Merck KGaA) or Sigma-Aldrich Chemicals (Sigma-Aldrich Corp.). The reactions and the purities of the compounds were observed by thin layer chromatography (TLC) on silica gel 60 F_{254} aluminum sheets obtained from Merck. Melting points of the synthesized compounds were recorded by MP90 digital melting point apparatus (Mettler Toledo) and were presented as uncorrected. ^{1}H NMR and ^{13}C NMR spectra (see the Supporting Information) were recorded by a Bruker 300 and 75 MHz digital FT-NMR spectrometer (Bruker Bioscience) in DMSO-d_6, respectively. In the NMR spectra, splitting patterns were designated as follows: s: singlet; d: doublet; t: triplet; m: multiplet. Coupling constants (*J*) were reported as Hertz. High-resolution mass

spectrometry (HRMS) studies were performed using an LC/MS-IT-TOF system (Shimadzu). The IR spectral analyses were achieved using Infrared Affinity-1S spectrophotometer with attenuated total reflectance (ATR) technology (Shimadzu-IR Affinity-1S).

The InChI codes of the investigated compounds, together with some biological activity data, are provided as Supporting Information.

4.1.2 | Synthesis of 4-thiomorpholinobenzaldehyde (1)

Thiomorpholine (2.06 g, 0.02 mol) was added to a solution of 4-fluorobenzaldehyde (2.48 g, 0.02 mol) in DMF (25 mL) at room temperature. The mixture was stirred for 24 h at 150°C. The reaction was monitored with TLC. After the reaction is completed, slowly pour the mixture into a glass of ice water. The precipitate was filtered off and washed with cold water. Yield: 79%.

4.1.3 | Synthesis of 2-(4-thiomorpholinobenzylidene) hydrazinecarbothioamide (2)

Hydrazine carbothioamide (0.91 g, 0.01 mol) was added to a solution of 4-thiomorpholinobenzaldehyde (**1**) (2.07 g, 0.01 mol) in ethanol (50 mL) at room temperature. The mixture was stirred for 3 h at 80°C. The reaction was monitored with TLC. After the reaction completed, precipitate was filtered off and washed with cold ethanol. Yield 84%.

4.1.4 | General synthesis of 4-(4-{[2-(thiazol-2-yl) hydrazone]methyl}phenyl)thiomorpholine derivatives (3a–3l)

2-Bromo-1-phenylethanone derivatives (1.30 mmol) were added to a solution of 2-(4-thiomorpholinobenzylidene)hydrazinecarbothioamide (**2**) (0.36 g, 1.30 mmol) in ethanol (50 mL). The mixture was stirred at 80°C. The reaction was monitored with TLC. After the reaction was completed, the product was filtered. The final products were recrystallized from ethanol.

4-(4-{2-[4-(4-Fluorophenyl)thiazol-2-yl]hydrazono}methyl) phenylthiomorpholine (**3a**): m. p. 215–216°C, yield 84%, ^{1}H-NMR (300 MHz, DMSO-d_6, ppm) δ 2.71 (brs, 4H, thiomorpholine-$\underline{C}_2$ and $\underline{C}_6$), 3.67 (brs, 4H, thiomorpholine-$\underline{C}_3$ and $\underline{C}_5$), 7.02–7.11 (m, 2H, Ar-H), 7.12–7.18 (m, 1H, Ar-H), 7.21–7.32 (m, 2H, Ar-H), 7.50–7.62 (m, 3H, Ar-H), 7.81–7.89 (m, 1H, Ar-H), 7.98–8.04 (m, 1H, Ar-H). ^{13}C-NMR (75 MHz, DMSO-d_6, ppm) δ 25.37 (thiomorpholine-$\underline{C}_2$ and $\underline{C}_6$), 51.43 (thiomorpholine-$\underline{C}_3$ and $\underline{C}_5$), 103.68, 115.79, 116.68, 128.14, 128.27, 129.33, 131.21, 142.71, 160.51, 163.75, 168.84. For $C_{20}H_{19}FN_4S_2$, HRMS (*m/z*): $[M+H]^+$ calculated 399.1108; found 399.1111. IR (cm^{-1}) *v*: 3050 (Ar–H), 2986, 2901 (Aliph C–H), 1622, 1506 (C=C, C=N), 1281, 1234, 1221, 1182, 1167, 1095, 1043 (C–O, C–N), 893, 837, 754, 708 (benzene ring out-of-plane deformation bands).

4-[4-({2-[4-(4-Chlorophenyl)thiazol-2-yl]hydrazono}methyl) phenyl]thiomorpholine (**3b**): m. p. 239–240°C, yield 89%, ^{1}H-NMR (300 MHz, DMSO-d_6, ppm) δ 2.67–2.70 (m, 4H, thiomorpholine-$\underline{C}_2$ and $\underline{C}_6$), 3.65–3.66 (m, 4H, thiomorpholine-$\underline{C}_3$ and $\underline{C}_5$), 7.03 (d, *J* = 8.85 Hz, 2H, Phenyl-H), 7.35 (s, 1H, thiazol-H), 7.46 (d, *J* = 8.62 Hz, 2H, chlorophenyl-H), 7.52 (d, *J* = 8.85 Hz, 2H, phenyl-H), 7.85 (d, *J* = 8.62 Hz, 2H, chlorophenyl-H), 7.95 (s, 1H, N–N=$\underline{CH}$). ^{13}C-NMR (75 MHz, DMSO-d_6, ppm) δ 25.40 (thiomorpholine-$\underline{C}_2$ and $\underline{C}_6$), 51.20 (thiomorpholine-$\underline{C}_3$ and $\underline{C}_5$), 104.56, 116.28, 127.71, 128.20, 129.08, 132.40, 133.81, 142.53, 149.27, 150.35, 168.91. For $C_{20}H_{19}ClN_4S_2$, HRMS (*m/z*): $[M+H]^+$ calculated 415.0812; found 415.0808. IR (cm^{-1}) *v*: 3072 (Ar-H), 2947, 2901 (Aliph C–H), 1622, 1601, 1556, 1402 (C=C, C=N), 1217, 1184, 1092, 1011 (C–O, C–N), 951, 891, 825, 752, 698 (benzene ring out-of-plane deformation bands).

4-[4-({2-[4-(4-Nitrophenyl)thiazol-2-yl]hydrazono}methyl) phenyl]thiomorpholine (**3c**): m. p. 226–227°C, yield 74%, ^{1}H-NMR (300 MHz, DMSO-d_6, ppm) δ 2.66–2.69 (m, 4H, thiomorpholine-$\underline{C}_2$ and $\underline{C}_6$), 3.65–3.68 (m, 4H, thiomorpholine-$\underline{C}_3$ and $\underline{C}_5$), 7.01 (d, *J* = 8.85 Hz, 2H, Phenyl-H), 7.52 (d, *J* = 8.85 Hz, 2H, phenyl-H), 7.68 (s, 1H, thiazol-H), 7.95 (s, 1H, N–N=$\underline{CH}$) 8.09 (d, *J* = 9.01 Hz, 2H, nitrophenyl-H), 8.27 (d, *J* = 9.03, 2H, nitrophenyl-H), 12.08 (brs, 1H, N–N–H). ^{13}C-NMR (75 MHz, DMSO-d_6, ppm) δ 25.41 (thiomorpholine-$\underline{C}_2$ and $\underline{C}_6$), 51.06 (thiomorpholine-$\underline{C}_3$ and $\underline{C}_5$), 108.64, 116.12, 124.58, 126.78, 128.22, 141.16, 142.67, 146.61, 148.87, 169.20. For $C_{20}H_{19}N_5O_2S_2$, HRMS (*m/z*): $[M+H]^+$ calculated 426.1053; found 426.1066. IR (cm^{-1}) *v*: 3082 (Ar-H), 2988, 2893 (Aliph C–H), 1624, 1597 (C=C, C=N), 1517, 1342 (NO2), 1281, 1219, 1107, 1047 (C–O, C–N), 957, 851, 814, 741, 692 (benzene ring out-of-plane deformation bands).

4-(4-{[2-(4-Phenylthiazol-2-yl)hydrazono]methyl}phenyl) thiomorpholine (**3d**): m. p. 213–214°C, yield 79%, ^{1}H-NMR (300 MHz, DMSO-d_6, ppm) δ 2.69–2.71 (m, 4H, thiomorpholine-$\underline{C}_2$ and $\underline{C}_6$), 3.67–3.71 (m, 4H, thiomorpholine-$\underline{C}_3$ and $\underline{C}_5$), 7.03–7.13 (m, 2H, Ar-H), 7.25–7.34 (m, 3H, Ar-H), 7.39–7.44 (m, 1H, Ar-H), 7.53–7.62 (m, 3H, Ar-H), 7.75–7.84 (m, 1H, Ar-H), 7.99–8.06 (m, 1H, N–N=$\underline{CH}$). ^{13}C-NMR (75 MHz, DMSO-d_6, ppm) δ 25.35 (thiomorpholine-C_2 and C_6), 51.70 (thiomorpholine-C_3 and C_5), 104.02. 116.79, 126.13, 127.35, 128.00, 128.36, 128.85, 129.12, 134.21, 143.13, 149.80, 168.75. For $C_{20}H_{20}N_4S_2$, HRMS (*m/z*): $[M+H]^+$ calculated 381.1202; found 381.1193. IR (cm^{-1}) *v*: 1620, 1597, 1518 (C=C, C=N), 1281, 1234, 1221, 1182, 1167, 1095, 1043 (C–O, C–N), 893, 837, 754, 708 (benzene ring out-of-plane deformation bands).

4-{2-[2-(4-Thiomorpholinobenzylidene)hydrazinyl]thiazol-4-yl} benzonitrile (**3e**): m. p. 219–220°C, yield 84%, ^{1}H-NMR (300 MHz, DMSO-d_6, ppm) δ 2.66–2.70 (m, 4H, thiomorpholine-$\underline{C}_2$ and $\underline{C}_6$), 3.65–3.68 (m, 4H, thiomorpholine-$\underline{C}_3$ and $\underline{C}_5$), 7.03 (d, *J* = 8.85 Hz, 2H, phenyl-H), 7.52 (d, *J* = 8.85 Hz, 2H, phenyl-H), 7.60 (s, 1H, thiazol-H), 7.86 (d, *J* = 8.61 Hz, 2H, benzonitrile-H), 7.96 (s, 1H, N–N=$\underline{CH}$), 8.02 (d, *J* = 8.52 Hz, 2H, benzonitrile-H), 12.05 (brs, 1H, N–N–H). ^{13}C-NMR (75 MHz, DMSO-d_6, ppm) δ 25.40 (thiomorpholine-C_2 and C_6), 51.15 (thiomorpholine-C_3 and C_5), 107.60, 109.98, 116.23, 119.47, 125.28, 126.56, 128.21, 133.15, 139.22, 142.59, 149.11, 150.42, 169.10. For

$C_{21}H_{19}N_5S_2$, HRMS (*m/z*): $[M+H]^+$ calculated 406.1155; found 406.1135. IR (cm^{-1}) *v*: 3064 (Ar-H), 2959 (Aliph C–H), 1597, 1522, 1404 (C=C, C=N), 1279, 1182, 1045 (C–O, C–N), 953, 837, 752, 706 (benzene ring out-of-plane deformation bands).

4-[4-({2-[4-(p-Tolyl)thiazol-2-yl]hydrazono}methyl)phenyl] thiomorpholine (**3f**): m. p. 185–186°C, yield 86%, ^{1}H-NMR (300 MHz, DMSO-d_6, ppm) δ 2.31 (s, 3H, toluene-CH_3), 2.65–2.68 (m, 4H, thiomorpholine-C_2 and C_6), 3.64–3.68 (m, 4H, thiomorpholine-C_3 and C_5), 7.00 (d, *J* = 8.87 Hz, 2H, phenyl-H), 7.20–7.22 (m, 3H, toluene Ar-H and thiazol-H), 7.51 (d, *J* = 8.86 Hz, 2H, phenyl-H), 7.52 (d, *J* = 8.13 Hz, 2H, toluene Ar-H), 7.95 (s, 1H, N–N=CH), 11.94 (brs, 1H, N–N–H). ^{13}C-NMR (75 MHz, DMSO-d_6, ppm) δ 21.27 (phenyl-CH_3), 25.42 (thiomorpholine-C_2 and C_6), 50.94 (thiomorpholine-C_3 and C_5), 102.83, 116.00, 125.97, 128.21, 129.64, 132.11, 137.38, 142.67, 150.66, 168.71. For $C_{21}H_{22}N_4S_2$, HRMS (*m/z*): $[M+H]^+$ calculated 395.1359; found 395.1354. IR (cm^{-1}) *v*: 2949, 2902 (Aliph C–H), 1620, 1599, 1518, 1396 (C=C, C=N), 1215, 1182, 1045 (C–O, C–N), 949, 891, 818, 806, 752, 710 (benzene ring out-of-plane deformation bands).

4-[4-({2-[4-(4-Methoxyphenyl)thiazol-2-yl]hydrazono}methyl) phenyl]thiomorpholine (**3g**): m. p. 141–142°C, yield 77%, ^{1}H-NMR (300 MHz, DMSO-d_6, ppm) δ 2.66–2.70 (m, 4H, thiomorpholine-C_2 and C_6), 3.65–3.68 (m, 4H, thiomorpholine-C_3 and C_5), 3.78 (s, 3H, phenyl-OCH_3), 6.79 (d, *J* = 8.82 Hz, 1H, Ar-H), 6.98 (d, *J* = 8.90 Hz, 2H, Ar-H), 7.03 (d, *J* = 8.80 Hz, 1H, Ar-H), 7.12 (s, 1H, thiazol-H), 7.19 (d, *J* = 8.79 Hz, 1H, Ar-H), 7.49–7.55 (m, 2H, Ar-H), 7.76 (d, *J* = 8.79 Hz, 1H, Ar-H), 8.00 (s, 1H, N–N=CH). ^{13}C-NMR (75 MHz, DMSO-d_6, ppm) δ 25.40 (thiomorpholine-C_2 and C_6), 51.16 (thiomorpholine-C_3 and C_5), 55.64 (phenyl-OCH_3), 101.78, 114.19, 114.46, 116.22, 127.11, 127.48, 128.33, 128.60, 129.13, 129.86, 143.20, 150.43, 159.43, 168.68. For $C_{21}H_{22}N_4OS_2$, HRMS (*m/z*): $[M+H]^+$ calculated 411.1308; found 411.1308. IR (cm^{-1}) *v*: 1600, 1558, 1508, 1387 (C=C, C=N), 1250, 1217, 1180, 1090, 1026 (C–O, C–N), 951, 891, 833 (benzene ring out-of-plane deformation bands).

4-[4-({2-[4-(3-Chlorophenyl)thiazol-2-yl]hydrazono}methyl) phenyl]thiomorpholine (**3h**): m. p. 189–190°C, yield 72%, ^{1}H-NMR (300 MHz, DMSO-d_6, ppm) δ 2.63–2.67 (m, 4H, thiomorpholine-C_2 and C_6), 3.60–3.64 (m, 4H, thiomorpholine-C_3 and C_5), 6.95–7.02 (m, 2H, Ar-H), 7.09–7.12 (m, 1H, Ar-H), 7.20–7.27 (m, 2H, Ar-H), 7.31–7.40 (m, 2H, Ar-H),7.44–7.53 (m, 2H, Ar-H), 7.94 (s, 1H, N–N=CH). ^{13}C-NMR (75 MHz, DMSO-d_6, ppm) δ 25.37 (thiomorpholine-C_2 and C_6), 50.90 (thiomorpholine-C_3 and C_5), 105.31, 116.00, 124.50, 125.66, 126.66, 128.19, 129.14, 130.51, 130.99, 133.54, 136.77, 143.14, 150.64, 166.47. For $C_{20}H_{19}ClN_4S_2$, HRMS (*m/z*): $[M+H]^+$ calculated 415.0812; found 415.0806. IR (cm^{-1}) *v*: 3302 (N–H), 3147 (Ar-H), 2995, 2814 (Aliph C–H), 1574, 1549, 1514, 1450, 1369 (C=C, C=N), 1273, 1209, 1180 (C–O, C–N), 993, 949, 872, 818, 698, 635 (benzene ring out-of-plane deformation bands).

4-[4-({2-[4-(3-Methoxyphenyl)thiazol-2-yl]hydrazono}methyl) phenyl]thiomorpholine (**3i**): m. p. 170–171°C, yield 80%, ^{1}H-NMR (300 MHz, DMSO-d_6, ppm) δ 2.70 (brs, 4H, thiomorpholine-C_2 and C_6), 3.44–3.77 (m, 7H, thiomorpholine-C_3 and C_5, and OCH_3), 4.86 (s, 3H, phenyl-OCH_3), 6.82–7.80 (m, 8H, Ar-H), 8.00–8.13 (m, 1H, N–N=CH). ^{13}C-NMR (75 MHz, DMSO-d_6, ppm) δ 25.31 (thiomorpholine-C_2 and C_6), 51.77 (thiomorpholine-C_3 and C_5), 55.31 (phenyl-OCH_3), 113.41, 113.66, 114.27, 114.91, 115.42, 116.11, 119.65, 128.40, 129.21, 129.87, 159.39. For $C_{21}H_{22}N_4OS_2$, HRMS (*m/z*): $[M+H]^+$ calculated 411.1308; found 411.1297. IR (cm^{-1}) *v*: 1595, 1520, 1489, 1429 (C=C, C=N), 1290, 1236, 1182, 1028 (C–O, C–N), 945, 891, 845, 787, 768 (benzene ring out-of-plane deformation bands).

4-[4-({2-[4-(3-Nitrophenyl)thiazol-2-yl]hydrazono}methyl)phenyl] thiomorpholine (**3j**): m. p. 197–198°C, yield 79%, ^{1}H-NMR (300 MHz, DMSO-d_6, ppm) δ 2.61–2.67 (m, 4H, thiomorpholine-C_2 and C_6), 3.66–3.79 (m, 4H, thiomorpholine-C_3 and C_5), 6.9–7.11 (m, 2H, Ar-H), 7.46–7.78 (m, 5H, Ar-H), 7.97–8.14 (m, 2H, Ar-H), 8.55–8.80 (m, 1H, N–N=CH). ^{13}C-NMR (75 MHz, DMSO-d_6, ppm) δ 25.27 (thiomorpholine-C_2 and C_6), 49.98 (thiomorpholine-C_3 and C_5), 113.23, 113.88, 114.76, 115.87, 122.79, 129.20, 130.41, 130.58, 132.24, 134.87, 136.03. For $C_{20}H_{19}N_5O_2S_2$, HRMS (*m/z*): $[M+H]^+$ calculated 426.1053; found 426.1062. IR (cm^{-1}) *v*: 1553 and 1344 (NO_2), 1512, 1435 (C=C, C=N), 1283, 1236, 1201, 1134, 1053, 1012 (C-O, C-N), 962, 908, 866, 835, 775, 752, 725, 682 (benzene ring out-of-plane deformation bands).

4-[4-({2-[4-(3-Fluorophenyl)thiazol-2-yl]hydrazono}methyl)phenyl] thiomorpholine (**3k**): m. p. 175–176°C, yield 81%, ^{1}H-NMR (300 MHz, DMSO-d_6, ppm) δ 2.61–2.64 (m, 4H, thiomorpholine-C_2 and C_6), 3.61–3.64 (m, 4H, thiomorpholine-C_3 and C_5), 6.94–6.97 (m, 2H, Ar-H), 7.07–7.12 (m, 2H, Ar-H), 7.19–7.26 (m, 2H, Ar-H), 7.42–7.50 (m, 2H, Ar-H), 7.61–7.71 (m, 1H, Ar-H), 7.93 (s, 1H, N–N=CH). ^{13}C-NMR (75 MHz, DMSO-d_6, ppm) δ 25.37 (thiomorpholine-C_2 and C_6), 50.85 (thiomorpholine-C_3 and C_5), 105.19, 112.32, 114.73, 115.03, 115.97, 124.17, 128.18, 129.10, 130.69, 143.10, 166.48. For $C_{20}H_{19}FN_4S_2$, HRMS (*m/z*): $[M+H]^+$ calculated 399.1108; found 399.1102. IR (cm^{-1}) *v*: 1599, 1514, 1357 (C=C, C=N), 1288, 1275, 1215, 1182, 1126, 1090, 1028 (C–O, C–N), 953, 889, 816, 750 (benzene ring out-of-plane deformation bands).

4-[4-({2-[4-(Naphthalen-2-yl)thiazol-2-yl]hydrazono}methyl)phenyl] thiomorpholine (**3l**): m. p. 117–118°C, yield 76%, ^{1}H-NMR (300 MHz, DMSO-d_6, ppm) δ 2.65–2.69 (m, 4H, thiomorpholine-C_2 and C_6), 3.65–3.68 (m, 4H, thiomorpholine-C_3 and C_5), 7.01 (d, *J* = 8.88 Hz, 2H, phenyl-H), 7.45 (s, 1H, thiazol-H), 7.49–7.55 (m, 4H, Ar-H), 7.89–8.02 (m, 5H, Ar-H), 8.37 (s, 1H, N–N=CH). ^{13}C-NMR (75 MHz, DMSO-d_6, ppm) δ 25.43 (thiomorpholine-C_2 and C_6), 50.98 (thiomorpholine-C_3 and C_5), 104.57, 116.05, 124.41, 124.54, 125.01, 126.49, 126.93, 128.05, 128.21, 128.56, 128.62, 132.39, 132.89, 133.60, 142.56, 150.63, 168.88. For $C_{24}H_{22}N_4S_2$, HRMS (*m/z*): $[M+H]^+$ calculated 431.1359; found 431.1354. IR (cm^{-1}) *v*: 3053 (Ar-H), 2903 (Aliph C–H), 1620, 1597, 1518, 1395 (C=C, C=N), 1275, 1215, 1182, 1090, 1041 (C–O, C–N), 952, 891, 853, 806, 748, 708 (benzene ring out-of-plane deformation bands).

4.2 | Biological activity

4.2.1 | Cell multiplication and preparation of cell culture

The lung cancer cell line (A549-ATCC® CCL-185™), and the healthy connective tissue cell line (L929) were multiplied in RPMI-1640 medium

as described in the literature.[35] The medium is composed of 10% fetal bovine serum (FBS), 1% penicillin/streptomycin, 1% L-glutamine, and 1% amphotericin-B. The cells were cultured in a 5% CO_2 oven at 95% relative humidity and 37°C. When the cell density in the culture vessel reached 70% (after approximately 2–3 days), they were divided into subcultures and allowed to grow. Part of the multiplied cells were stored at −80°C for future experiments regarding our current study.

L929 cells were prepared by incubating in 25 cm^2 flasks containing Dulbecco's Modification of Eagles (DMEM) media containing 10% FBS, 0.2 mM glutamine, 100 IU/mL penicillin, and 1% g/mL streptomycin in a 95% air and 5% CO_2 gas environment at 37°C.

4.2.2 | Cytotoxicity assay (MTT method)

Cells that have reached the 80% growth phase are collected with 0.25% trypsin/EDTA solution and counted by hemocytometry.[35] Cells are suspended at a concentration of 2×10^4 cells/mL. Solutions of test substances prepared at different concentrations in dimethylsulfoxide (DMSO) are added to the cell suspension and 200 µL of cell suspension is seeded into 96-well plates, using three wells for each concentration. Cells are incubated at 37°C for 24 h. At the end of the incubation period, 20 µL of MTT dye (3-(4,5-dimethylthiazol-2-yl)-2,5-diphenyltetrazolium bromide) is added to the cells and incubated for another 2 h at 37°C. At the end of this period, the MTT dye taken up by the cells is dissolved in DMSO and absorbance measurement is performed at 540 nm with an Elisa spectrometer.

4.2.3 | In vitro matrix metalloproteinase-9 (MMP-9) Inhibition

The MMP-9 inhibition was evaluated according to the method in our previous study.[36] MMP Colorimetric Drug Discovery Kits are a complete assay system designed to screen for MMP inhibitors using a thiopeptide as a chromogenic substrate (Ac-PLG-[2-mercapto-4-methyl-pentanoyl]-LG-OC_2H_5). The MMP cleavage site peptide bond is replaced with a thioester bond in the thiopeptide. Hydrolysis of this bond by an MMP produces a sulfhydryl group that reacts with DTNB [5,50-dithiobis (2-nitrobenzoic acid), Ellman's reagent] to form 2-nitro-5-iobenzoic acid, which can be detected by its absorbance at 412 nm. Assays are performed in triplicate. UV absorbance is read at 412 nm using a microplate reader (BioTek, PowerWave, Gen5 software) at room temperature. NNGH is used as a control inhibitor. Data are expressed as Mean ± SD. The % inhibitory activity of MMPs was calculated using the following equation:

$$\%\text{Inhibitory activity} = (V_{\text{inhibitor}}/V_{\text{control}}) \times 100.$$

Inhibition of MMPs percentage was calculated using the following equation:

$$\text{I}(\%) = 100 - \%\text{inhibitory activity}.$$

4.3 | ADME parameters

Certain descriptors of ADME were calculated by in silico means using SwissADME tool. The predicted properties included the number of HBD, number of HBA, TPSA, Log P, Log S, absorption through the gastrointestinal tract (GIA), Log K_p, drug-likeness by calculating the number of violations of Lipinski's rule of five (RoF), ease of chemical synthesis described by the synthetic accessibility (SA).

4.4 | DFT calculations

Theoretical investigations were conducted on the most active compounds **3c**, **3d**, **3f**, and **3g** utilizing the Gaussian 09 W software package[37] and GaussView 5.0 molecular visualization program.[38] The optimization of the compounds' geometry was executed in the ground state and gas phase using DFT with Becke's Three-Parameter Hybrid Functional and the Lee, Yang, and Parr correlation (B3LYP) method,[39] employing the 6–31 G(d,p) basis set.

To elucidate intramolecular charge–transfer interactions, the highest occupied molecular orbital (HOMO) and lowest unoccupied molecular orbital (LUMO) energy values of the compound groups were determined through time-dependent (TD)-DFT calculations. These energy values were utilized to derive various chemical activity parameters, including ionization potential ($I = -$EHOMO), electron affinity (A = −ELUMO), electronegativity ($\chi = (I + A)/2$), chemical hardness ($\eta = (I - A)/2$), chemical softness ($S = 1/2\eta$), chemical potential ($\mu = -(I + A)/2$), and electrophilicity index ($\omega = \mu 2/2\eta$) of the molecular groups.[35,40–43]

4.5 | Molecular docking and MDS studies

Molecular docking studies were performed to define the binding modes of the active compounds in the active regions of the MMP-9 enzyme complex X-ray crystal structure (PDB ID: 5I12) which was retrieved from the Protein Data Bank server (www.pdb.org, accessed May 01, 2018). Schrödinger's Maestro interface and its applications (LigPrep and Glide modules) were used for the molecular docking study.[44] Using the docking pose, an MDS study was performed according to the Maestro Desmond interface program Schrodinger Release 2020-3.[44] MDS was carried out at 100 ns. The stability analysis of the identified hits was run. Preparing the system setup, performing MDS, and computing the interaction analysis were achieved according to similar procedures in the literature.[36,45,46] All systems were configured using the "System Builder" module. The complex structure underwent energy minimization using the OPLS3e standard force field. Transferable intermolecular potential with the 3-point water (TIP3P) model was utilized for the composition of the hydration model. Neutralization of the system was achieved using Na^+ and Cl^- ions. The MDS study was conducted after the system setup was completed. The applied docking and dynamics simulation procedures were carried out following previously published work.[32]

ACKNOWLEDGMENTS

This study was supported by the Anadolu University Scientific Research Project, Eskisehir, Turkey (Project no. 2105S098). The MDS video can be found in https://youtu.be/QLCHnH-2eDo.

CONFLICTS OF INTEREST STATEMENT

The authors declare no conflicts of interest.

DATA AVAILABILITY STATEMENT

The data that support the findings of this study are available in the supplementary material of this article.

ORCID

Sam Dawbaa http://orcid.org/0000-0001-7001-0739
Asaf Evrim Evren http://orcid.org/0000-0002-8651-826X
Demokrat Nuha http://orcid.org/0000-0002-7271-6791
Leyla Yurttaş http://orcid.org/0000-0002-0957-6044

REFERENCES

[1] K. Buran, *Saglik Bilim. Enstitüsü* **2013**.
[2] N. Aydemir, R. Bilaloğlu, *Mutat. Res. Genet. Toxicol. Environ. Mutagen.* **2003**, *537*, 43.
[3] W. O. Foye, Lippincott Williams & Wilkins, Shawnee Mission, KS **1995**.
[4] M.-L. Zhu, C.-Y. Wang, C.-M. Xu, W.-P. Bi, X.-Y. Zhou, *Int. Med. J. Exp. Clin. Res.* **2017**, *23*, 1146.
[5] A. E. Evren, L. Yurttaş, B. Ekselli, G. Akalın-Cıftcı, *Lett. Drug Des. Discovery* **2019**, *16*, 547.
[6] A. E. Evren, L. Yurttas, B. Ekselli, G. Akalin-Ciftci, *Phosphorus. Sulfur. Silicon. Relat. Elem.* **2019**, *198*, 820.
[7] A. E. Evren, D. Nuha, S. Dawbaa, B. N. Sağlık, L. Yurttaş, *Eur. J. Med. Chem.* **2022**, *229*, 114097.
[8] A. E. Evren, S. Dawbaa, D. Nuha, A. Z. Kaya, Z. Canturk, L. Yurttacs, *Kocatepe Vet. J.* **n.d.**, *17*, 104.
[9] S. Dawbaa, A. E. Evren, Z. Cantürk, L. Yurttaş, *Phosphorus Sulfur Silicon Relat. Elem.* **2021**,1.
[10] A. E. Evren, S. Dawbaa, D. Nuha, A. Yavuz, Ü. D. Gül, L. Yurttaş, *J. Mol. Struct.* **2021**,130692.
[11] S. R. Alizadeh, S. M. Hashemi, *Med. Chem. Res.* **2021**, *30*, 771.
[12] A.-M. Borcea, I. Ionuț, O. Crișan, O. Oniga, *Molecules* **2021**, *26*, 624.
[13] A. Singh, D. Malhotra, K. Singh, R. Chadha, P. M. S. Bedi, *J. Mol. Struct.* **2022**, *1266*, 133479.
[14] T. A. Farghaly, A. M. R. Alsaedi, N. A. Alenazi, M. F. Harras, *Expert Opin. Ther. Pat.* **2022**, *32*, 791.
[15] J. Chen, J. Stubbe, *Nat. Rev. Cancer* **2005**, *5*, 102.
[16] L. V. Arsenie, V. Ladmiral, P.-L. Desmazes, S. Catrouillet, *Eur. Polym. J.* **2023**,112490.
[17] A. Kumari, R. K. Singh, *Bioorg. Chem.* **2020**, *96*, 103578.
[18] S. Karunanidhi, B. Chandrasekaran, R. Karpoormath, H. M. Patel, F. Kayamba, S. R. Merugu, V. Kumar, S. Dhawan, B. Kushwaha, M. C. Mahlalela, *Bioorg. Chem.* **2021**, *115*, 105133.
[19] P.-C. Diao, Q. Li, M.-J. Hu, Y.-F. Ma, W.-W. You, K. H. Hong, P.-L. Zhao, *Eur. J. Med. Chem.* **2017**, *134*, 110.
[20] T. A. Hill, S. G. Stewart, B. Sauer, J. Gilbert, S. P. Ackland, J. A. Sakoff, A. McCluskey, *Bioorg. Med. Chem. Lett.* **2007**, *17*, 3392.
[21] A. Hiranrat, D. C. Holland, W. Mahabusarakam, J. N. A. Hooper, V. M. Avery, A. R. Carroll, *Mar. Drugs* **2021**, *19*, 95.
[22] L. Mezil, C. Berruyer-Pouyet, O. Cabaud, E. Josselin, S. Combes, J.-M. Brunel, P. Viens, Y. Collette, D. Birnbaum, M. Lopez, **2012**.
[23] G. Chauvière, B. Bouteille, B. Enanga, C. de Albuquerque, S. L. Croft, M. Dumas, J. Périé, *J. Med. Chem.* **2003**, *46*, 427.
[24] "SwissADME Web Tool," http://www.swissadme.ch/index.php
[25] C. A. Lipinski, F. Lombardo, B. W. Dominy, P. J. Feeney, *Adv. Drug Delivery Rev.* **1997**, *23*, 3.
[26] P. Politzer, J. S. Murray, *Theor. Chim. Acta* **2002**, *108*, 134.
[27] F. J. Luque, M. Orozco, P. K. Bhadane, S. R. Gadre, *J. Phys. Chem.* **1993**, *97*, 9380.
[28] H. Laronha, J. Caldeira, *Cells* **2020**, *9*, 1076.
[29] H.-J. Ra, W. C. Parks, *Matrix Biol.* **2007**, *26*, 587.
[30] G. A. Cabral-Pacheco, I. Garza-Veloz, C. la Rosa, J. M. Ramirez-Acuña, B. A. Perez-Romero, J. F. Guerrero-Rodriguez, N. Martinez-Avila, M. L. Martinez-Fierro, *Int. J. Mol. Sci.* **2020**, *9739*, 21.
[31] L. Yurttas, A. Evren, A. Kubilay, H. TEMEL, *ACTA Pharm. Sci.* **2021**, *59*.
[32] L. Yurttas, A. E. Evren, H. AlChaib, H. E. Temel, G. Akalin Çiftçi, *J. Biomol. Struct. Dyn.* **2023**,1.
[33] T.S., Rush, III, R. Powers, *Curr. Top. Med. Chem.* **2004**, *4*, 1311.
[34] G. LeDour, G. Moroy, M. Rouffet, E. Bourguet, D. Guillaume, M. Decarme, H. ElMourabit, F. Augé, A. J. Alix, J.-Y. Laronze, others, G. Bellon, W. Hornebeck, J. Sapi, *Bioorg. Med. Chem.* **2008**, *16*, 8745.
[35] D. Nuha, A. E. Evren, Z. Çiyanci, H. E. Temel, G. Akalin Çiftçi, L. Yurttas, *Arch. Pharm.* **2022**, *355*, 2200105.
[36] A. E. Evren, B. Ekselli, L. Yurttaş, H. E. Temel, G. Akalin Çiftçi, *J. Mol. Struct.* **2025**, *1320*, 139732.
[37] R. A. Gaussian09, *Inc., Wallingford CT* **2009**, *121*, p. 150.
[38] R. Dennington, T. Keith, J. Millam. Shawnee Mission, KS **2009**.
[39] A. D. Becke, *J. Chem. Phys.* **1992**, *96*, 2155.
[40] S. Dawbaa, D. Nuha, A. E. Evren, M. Y. Cankiliç, L. Yurttaş, G. Turan, *J. Mol. Struct.* **2023**, *1282*, 135213.
[41] D. Nuha, A. E. Evren, Ö. Kapusiz, Ü. D. Gül, N. Gundogdu-Karaburun, A. Ç. Karaburun, H. Berber, *J. Mol. Struct.* **2023**, *1272*, 134166.
[42] A. E. Evren, D. Nuha, L. Yurttaş, *Eur. J. Life Sci.* **2023**, *1*, 118.
[43] D. Nuha, H. Berber, A. Ç. Karaburun, **2022**.
[44] Schrodinger, Maestro Suite **2020**. https://www.schrodinger.com/platform/products/maestro/
[45] S. Dawbaa, C. Türkecs, D. Nuha, Y. Demir, A. E. Evren, L. Yurttacs, S. Ü. Beydemir, *J. Biomol. Struct. Dyn.* **2024**, 1.
[46] S. Saffour, A. E. Evren, B. N. Saglik, L. Yurttas, *Curr. Med. Chem.* **2024**.

SUPPORTING INFORMATION

Additional supporting information can be found online in the Supporting Information section at the end of this article.

How to cite this article: S. Dawbaa, A. E. Evren, D. Nuha, H. E. Temel, G. A. Çiftçi, L. Yurttaş, *Arch. Pharm.* **2025**, *358*, e2400821. https://doi.org/10.1002/ardp.202400821